Bulgarian Journal of Physics vol. **48** (2021) 1–11

Influence of Chromium Doping on Electrical and Elastic Behavior of $Nd_{0.5}Sr_{0.5}MnO_3$ System

Ashok Kumar Kusuma[1,3], **Elle Sagar**[1,2], **G. Sreeram Reddy**[2] **K. Vijaya Kumar**[1]

[1]Department of Physics, JNTU Hyderabad, Kukatpally, Hyderabad, 500 085, Telangana, India
[2]Vidya Jyothi Institute of Technology, Aziz Nagar Gate, Hyderabad, 500 075, Telangana, India
[3]B V Raju Institute of Technology, Narsapur, 502 313, Telangana, India

Received *03 January 2021*, Revised *07 January 2021*

Abstract. With a view to understand the influence of chromium doping at Mn site on electrical and elastic behavior of $Nd_{0.5}Sr_{0.5}MnO_3$ manganite system, a series of samples were prepared by the citrate sol–gel route method. The samples were characterized structurally by XRD and FTIR. The morphology of the samples was studied using scanning electronic microscope. A systematic investigation of electrical resistivity over a temperature range 4–300 K was carried out mainly to understand their magneto transport behavior in these materials. Except parent compound all the samples are found to have insulator to metal transitions. Later, the ultrasonic longitudinal (V_l) and shear wave (V_s) velocities were measured by the pulse transmission technique. Using the longitudinal (V_l) and shear (V_s) velocities, the elastic moduli were calculated. As the materials are porous, zero porous elastic moduli have been computed using Hasselmann and Fulrath model. It is observed that the elastic moduli of samples are found to increase continuously with increasing the concentration of the doping element and the observed variation of elastic moduli has been explained qualitatively.

KEY WORDS: CMR materials; Resistivity; Ultrasonic Velocity; Elastic modulii.

1 Introduction

Colossal magneto resistance (CMR) is a property of some materials, mostly manganese-based perovskite oxides, that enables them to dramatically change their electrical resistance in the presence of a magnetic field. Thus CMR materials attracted research community due to their interesting and effective behavior exhibited by them in structural, magnetic and electrical transport properties and their potential applications in memory devices [1–3]. The charge-ordered phase in half-doped manganites, with compositions, $RE_{0.5}A_{0.5}MnO_3$ (RE = La, Pr,

Sm, and Nd; A = Sr and Ca) exhibits a variety of phenomena such as charge, orbital, and spin ordering, along with electric and magnetic field induced transitions [4, 5]. Moreover, the charge ordered (CO)/orbital ordered (OO) and antiferromagnetic insulating (AFMI) phases can be modify effectively by doping at Mn site. In fact, Mn site substitutions with Cr in manganites have attracted great attention as Cr^{3+} ion is iso-electronic with Mn^{4+} ion. Magnetic impurities such as Cr and Ru can induce both metallicity and ferromagnetism in the insulating antiferromagnetic $Nd_{0.5}A_{0.5}MnO_3$ (A = Ca,Sr) [6, 7].

Further, large stresses can be developed in ceramic perovskites when they subjected to a high magnetic/electric field. Therefore, it is always useful to have a general idea of elastic moduli values that represent mechanical strength, fracture toughness and thermal shock resistance [8]. The velocity of longitudinal and transverse elastic waves thus produced is a characteristic feature of the solid. The most conventional technique for determination of elastic constants is the ultrasonic pulse transmission technique [9]. In view of this, electrical and elastic properties have been undertaken on Cr doped $Nd_{0.5}Sr_{0.5}Mn_{1-x}Cr_xO_3$ (x $=$ 0, 0.1, 0.2, 0.3 & 0.4) system.

2 Experimental Details

Polycrystalline $Nd_{0.5}Sr_{0.5}Mn_{1-x}Cr_xO_3$ (x $=$ 0, 0.1, 0.2, 0.3 & 0.4) samples were prepared by the sol–gel method [10] using pure metal nitrates as the starting materials (99.99% pure). The compositions of the samples are hereafter designated as NSMCO-0, NSMCO-1, NSMCO-2, NSMCO-3 and NSMCO-4, respectively. The powders were calcined at 1100°C for 8 h followed by sintering at 1300°C for 4 h in air. The structural characterization was carried out by powder X-ray diffraction (XRD) using Phillips expert diffractometer at room temperature in the 2θ range of 20–80°. The bulk densities of all the samples are measured using immersion method. By using bulk densities and X-ray densities, the porosity values has been calculated. The temperature vs resistivity measurements are undertaken using four probe method in the temperature range 4 K – 300 K.

The longitudinal and shear wave velocity measurements were also undertaken by using ultrasonic pulse transmission technique [11]. For this purpose, a pulse generator RPR-4000 (RITEC INC., USA) has been used. The pulse oscillator will generate RF pulses and a transmitting transducer then convert these pulses into acoustic pulses. These pulses in turn, after propagating through the test sample, which is in disc shape with thickness of $\sim$ 2.5 mm and with diameter of 10 mm, are converted into electrical signals by the receiving transducer. The amplified output signal was then displayed on a storage oscilloscope. Ultrasonic pulses were generated and detected by using X- and Y-cut (for longitudinal and shear waves respectively) 1 MHz quartz transducers. The transmission time of the ultra sound was measured up to an accuracy of 1 μs using a 100 MHz digital

storage oscilloscope (Tektronix model: TDS2012C). The overall accuracy of these measurements is about 0.25% in velocity and about 0.5% in elastic moduli.

3 Results and Discussions

3.1 Structural characterization

3.1.1 X-Ray diffraction

XRD studies were used for the structural investigation of the samples and the powder diffraction patterns of the samples are shown in Figure 1(a). A sys-

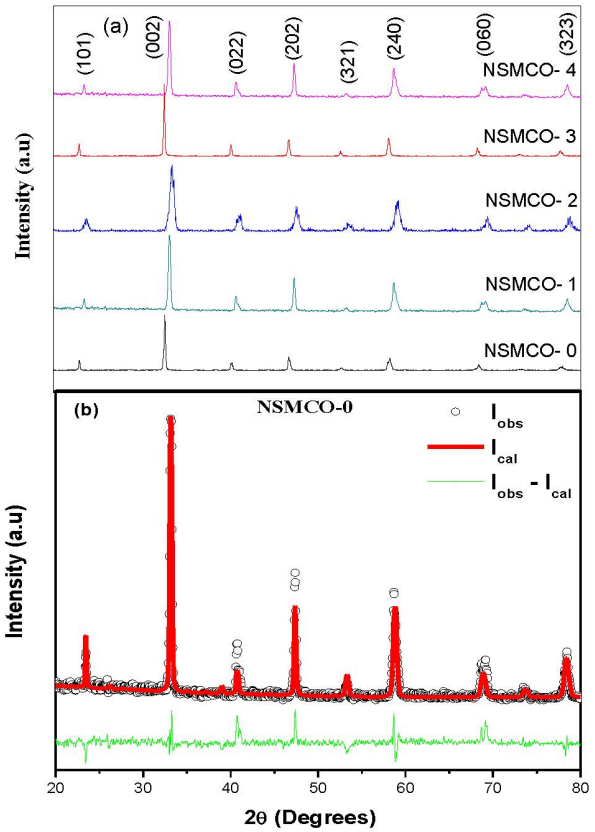

Figure 1. (a) XRD patters of Cr doped $Nd_{0.5}Sr_{0.5}MnO_3$ system; (b) Reitveld refined XRD pattern of NSMCO-0 sample. Circles indicate experimental points while red line indicates refined data and the green line indicates difference between experimental and refined data.

Table 1. Crystallographic data of Cr doped $Nd_{0.5}Sr_{0.5}MnO_3$ system

	Sample code				
Parameter	NSMCO-0	NSMCO-1	NSMCO-2	NSMCO-3	NSMCO-4
a (Å)	5.4301	5.4285	5.4292	5.4300	5.4296
b (Å)	7.6382	7.6425	7.6365	7.6450	7.6385
c (Å)	5.4622	5.4628	5.4615	5.4622	5.4630
R_P (%)	15.13	15.07	15.06	13.97	14.25
R_{WP} (%)	19.32	19.46	19.50	18.61	18.25
R_{EXP} (%)	18.78	18.52	18.78	18.11	18.16
Goodness of fit (S)	1.03	1.05	1.04	1.03	1.03

tematic analysis of the XRD data clearly reveals that all the samples are having single phase without any detectable impurity. Rietveld refinement technique [12, 13] was used to analyze the XRD data by assuming orthorhombic structure (*Pnma* space group). The Rietveld refinement fitted graph of NSMO-0 sample is shown as a representative of the samples in Figure 1(b). The fitted parameters of all the samples of the present investigation are given in Table 1. It can be seen from the table that there is no systematic variation in the lattice parameters with the Cr doping and the same behavior was reported earlier [14]. This may be attributed to the fact that there is a little difference between the ionic radii of $Cr^{3+}$and Mn^{3+} [15].

3.1.2 Scanning electron microscopy

The micro structural investigation of all the samples of the present investigation was carried out using a Scanning Electron Microscope and the micrographs of the samples are shown in Figure 2. From the micrographs it is clearly shown

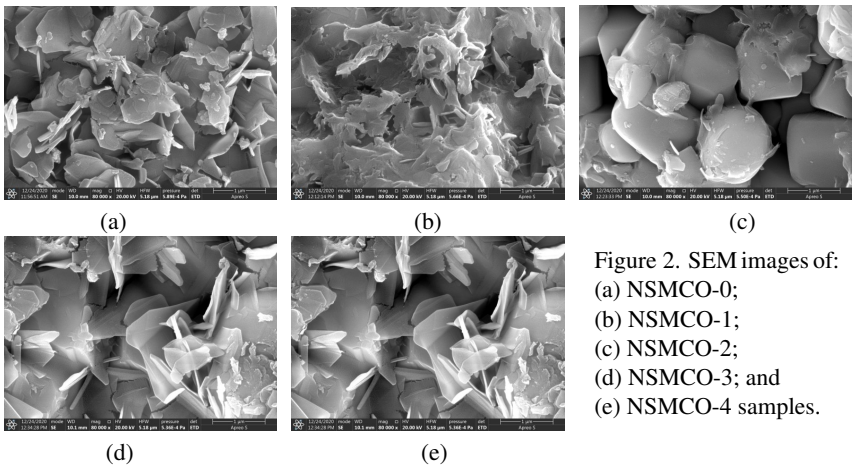

(a) (b) (c)

(d) (e)

Figure 2. SEM images of:
(a) NSMCO-0;
(b) NSMCO-1;
(c) NSMCO-2;
(d) NSMCO-3; and
(e) NSMCO-4 samples.

that the grain sizes of parent compound NSMCO-0 are in the range of 500 nm – 1 μm. It can also be seen from the micrographs that the shape of the grains of parent compound is not having any particular pattern. It is interesting to note that with increasing Chromium content, the grain size is also increased. Moreover for the samples NSMCO-2 and NSMCO-4, the grains are found to have circular shape.

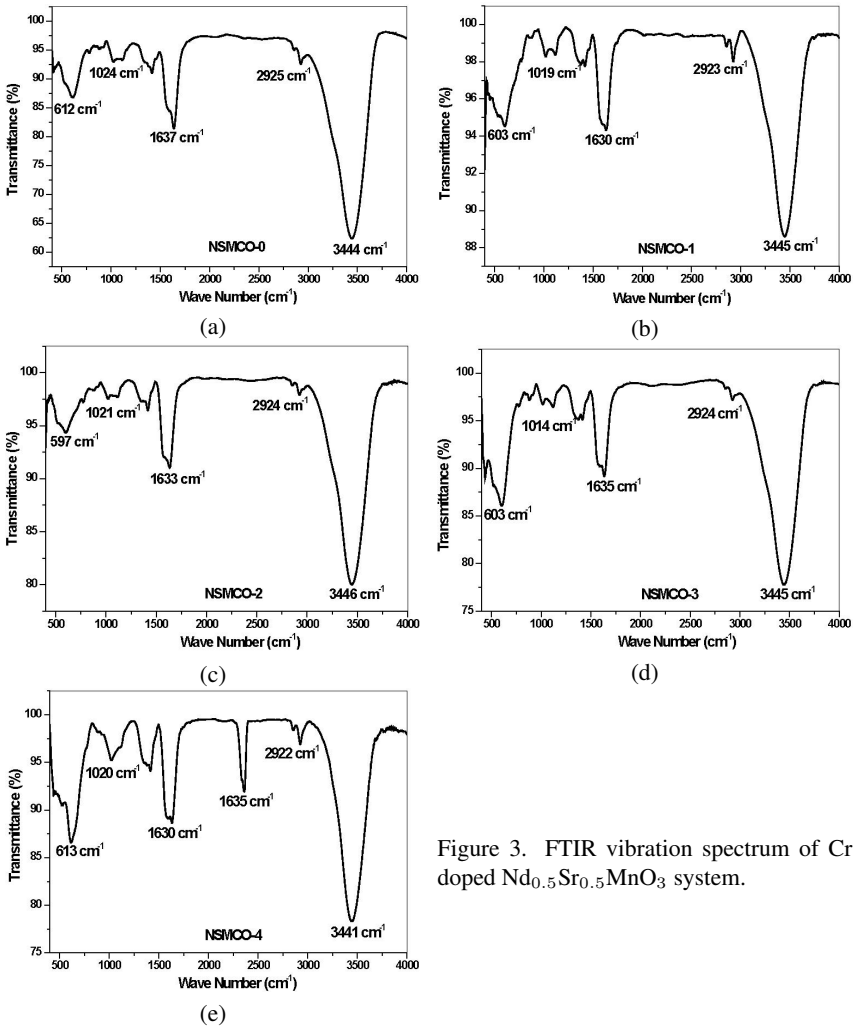

Figure 3. FTIR vibration spectrum of Cr doped $Nd_{0.5}Sr_{0.5}MnO_3$ system.

3.1.3 FTIR spectra

The chemistry for the formation any perovskite materials can be explained by studying the FTIR transmission spectra. The FTIR transmission spectra of Cr doped NSMO samples are presented in Figure 3. The absorption band around varying from 597 cm^{-1} to 613 cm^{-1} corresponds to stretching of the metal–oxygen bond in the perovskite, which involves the internal motion of a change in Mn–O–Mn bond length in MnO_6 octahedral. The broad absorption peak around 3450 cm^{-1} is the characteristic of absorbed water or hydroxyl group in the alco-

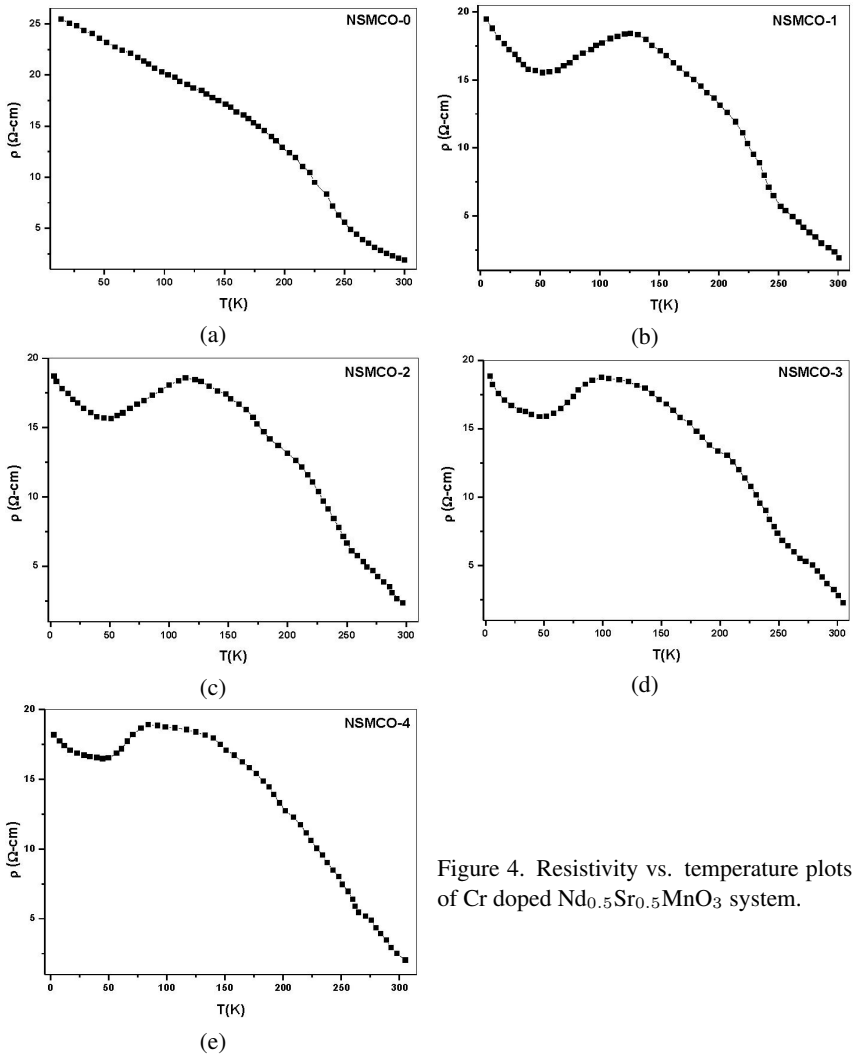

Figure 4. Resistivity vs. temperature plots of Cr doped $Nd_{0.5}Sr_{0.5}MnO_3$ system.

hol. A band around 1020 cm^{-1} reveals the formation of CH_3-CH_3-, CH_3-NH_2-, CH_3O- bands when the polymerization takes place with metal nitrate, citric acid, and ethylene glycol. This band at 1020 cm^{-1} can also be attributed to the C–C–O structure of ethylene glycol which was used in the polymerization process.

3.2 Electrical behavior

To understand the variation of electrical resistivity with temperature and the varying dopent concentration, resistivity measurements of the samples were undertaken in the temperature range 4–300 K and the results of those measurements are presented in Figure 4. It can be seen from the figure that the resistivity values of un doped sample is found to increase with decreasing temperature without having any transition exhibiting an insulating behavior throughout the temperature region of the investigation. This behavior of un doped sample is consistent with earlier reports [14]. In contrast, the resistivity values of chromium-doped samples are increasing with decreasing temperature up to $\sim$ 126 K exhibiting an insulating behavior. On further decrease of temperature, the resistivity values of Chromium doped samples after reaching a maximum are found to decrease indicating a metallic behavior. Thus exhibiting a metallic nature along with an upturn in the electrical properties is an interesting phenomenon exhibited by the doped samples of the present investigation. The T_P values of all the samples obtained from the resistivity versus temperature plots are found to decrease from 126 K to 85 K (Table 2) with increasing Cr content and the observed behavior may be explained as follows.

The transport properties of a manganite system may be explained on the basis of the electronic structure of the doping element, chromium. The ionic radii of Cr^{3+}, Mn^{3+}, and Mn^{4+} are 0.615, 0.645 and 0.530 Å respectively. As the ionic radius of Cr^{3+} and Mn^{3+} ions is nearly same, the doped Cr^{3+} ions can easily replace Mn^{3+}. Further, just as that Mn^{3+} and Mn^{4+} are having Ferro magnetic double exchange (FMDE) interaction, Cr^{3+} is also having similar FMDE interaction with Mn^{4+} and electronic configuration ($t_{2g}3$) as that of Mn^{4+}. By doping with Cr ions, the Mn^{3+}/Mn^{4+} ratio decreases and it is also known that Cr^{3+}–Mn^{3+} FMDE interaction is smaller than that of Mn^{3+}–Mn^{4+}. Finally, the

Table 2. Insulator to metal transition temperature, Porosity percentage and Ultrasonic velocities of Cr doped $Nd_{0.5}Sr_{0.5}$ MnO_3 system

Sample code	T_P (K)	Porosity %	V_l (m/s)	V_s (m/s)	σ	θ_D
(NSMCO-0)	—	14	4787	2776	0.24	457.5
(NSMCO-1)	126	11.7	5142	2776	0.29	454.8
(NSMCO-2)	114	14.57	5344	2884	0.29	461.0
(NSMCO-3)	99	12.55	5571	3064	0.28	491.3
(NSMCO-4)	84	12.86	5833	3353	0.25	537.2

effective FMDE interaction becomes weaker by doping with Cr which resulting in the gradual decrease of T_{P} with increasing Cr concentration [13].

3.3 Ultrasonic velocity studies

The longitudinal (V_l) and shear wave velocity (V_s) values of all the samples are presented in Table 2. The longitudinal as well as shear wave velocities are found to increase with increasing of concentration of doping element, and the observed behavior is in consistence with earlier reports of some other CMR materials [16] and manganites [8]. With the help of velocity values, Poisson's ratios (σ) of all the samples were calculated using the well-known relation [8],

$$\sigma = \frac{V_l^2 - 2V_s^2}{2(V_l^2 - V_s^2)} \tag{1}$$

and the values are given in Table 2. Further, Poisson's ratio values are found to vary in the range, 0.24–0.29 for different compositions. Finally, the elastic moduli values were also calculated using the well-known formulae [17] and the values are given in Table 3. Except for the sample NSMCO-1, both the elastic moduli (Young's modulus and rigid moduli) are found to increase with the doping concentration of doping ion and the same behavior of increasing elastic moduli with the doping concentration was observed earlier in some other CMR materials [16, 18].

3.4 Porosity correction

The well-known ceramic technique was used to prepare the materials of present investigation; as such they are ceramic in nature. In these types of ceramic materials, the strength of the samples depends on the percentage of porosity [8]. While discussing about the elastic behavior of the samples, it is essential to calculate the porosity values. With the help of bulk and X-ray densities the porosity values of all the samples are calculated and are presented in Table 2. The porosity percentage of all the samples is found to have in the range of 11–14%. As all the samples are found to have porosity, it is essential to correct the

Table 3. Elastic constants of Cr doped $Nd_{0.5}Sr_{0.5}$ MnO_3 system before and after porosity corrections

Sample	Before porosity correction		After porosity correction	
	E (GPa)	G (GPa)	E_0 (GPa)	G_0 (GPa)
(NSMCO-0)	106.39	42.90	147.9	59.18
(NSMCO-1)	105.00	40.70	148.34	56.49
(NSMCO-2)	118.00	45.74	154.17	58.98
(NSMCO-3)	129.12	50.44	172.55	66.54
(NSMCO-4)	149.35	59.74	201.25	79.82

elastic moduli to zero porosity so that the moduli are having some significance [8, 16]. For this purpose, Hasselman and Fulrath model has been used [19]. This model developed on the assumption that the samples prepared by ceramic process (sintered) contain mainly spherical type of pores. According to this model [19], Young's and shear wave moduli may be given by,

$$E_0 = \frac{E}{1-\alpha_E P}\,, \quad \text{where } \alpha_E = \frac{3(9+5\sigma)(1-\sigma)}{2(7-5\sigma)}\,, \tag{2}$$

$$G_0 = \frac{G}{1-\alpha_G P}\,, \quad \text{where } \alpha_G = \frac{15(1-\sigma)}{(7-5\sigma)}\,, \tag{3}$$

where E_O and G_O are the Young and rigidity moduli of non-porous matrix respectively, while E and G are the experimental values of Young's and rigidity moduli respectively, and P is porosity of the material. By using equations 2 and 3, porosity corrections have been made for the experimental elastic moduli and the zero porous values are given in Table 3.

From Table 3, one may see that the values of young's moduli values are found to increase continuously. A continuous increase in the elastic moduli with increase in doping concentration is in conformity with the behavior reported earlier in the case of some other manganites [16, 18]. Surprisingly, this linear behavior of increasing elastic module with doping concentration is missed in the case of rigidity module.

3.5 Acoustic Debye temperature (θ_{D}) values

Acoustic Debye temperature (θ_{D}) provides useful information about the physical properties of solids in general and CMR materials in particular. The Debye temperatures of all the samples of the present investigation have been calculated using Anderson's relation [20]

$$\text{Debye temperature:} \quad \theta_{\mathrm{D}} = \frac{h}{k}\left[\frac{3N_{\mathrm{A}}}{4\pi V_A}\right]^{1/3} V_m\,, \tag{4}$$

where h and k are Planck's and Boltzmann's constants respectively, N_{A} is the Avogadro number and V_A is the mean atomic volume given by $(M/\rho)/q$, where M is the molecular weight and q is the number of atoms in the formula unit and V_m is the average sound velocity calculated using the formula [20]

$$\text{Mean sound velocity:} \quad V_m = \left[\frac{3V_l^3 V_s^3}{V_s^3 + 2V_l^3}\right]^{1/3}. \tag{5}$$

The computed values of the acoustic Debye's temperature (θ_{D}) are given in Table 3 and are found to increase continuously with doping concentration.

4 Conclusions

1. CMR materials with compositional formula $Nd_{0.5}Sr_{0.5}Mn_{1-x}Cr_xO_3$(x = 0, 0.1, 0.2, 0.3 & 0.4) were synthesized without any detectable impurity and there is no systematic variation in the lattice parameters with the Cr doping is observed.

2. The samples are found to have different grain shapes with varying size from 500 nm to few micro meters.

3. The T_P values of all the samples obtained from the resistivity versus temperature plots are found to decrease from 136 K to 120 K with increasing Cr content.

4. Ultrasonic Longitudinal and shear wave velocities are found to increase with increasing Cr concentration.

5. The zero porous elastic moduli are found to increase continuously with increasing Cr concentration except for NSMCO-1 sample and the same behavior observed in the case of the Acoustic Debye temperatures (θ_D).

6. It is clearly observed that the mechanical strength of the samples was found to be increased with the Cr concentration.

Acknowledgements

The authors thank the TEQIP, JNTUH, Hyderabad & the Registrar, JNTUH, Hyderabad, for funding this work under the project of JNTUH/TEQIP-III/CRS/2019/MECH/02. The authors also thank, Dr. P. Venugopal Reddy, Vidya Jyothi Institute of Technology, Hyderabad, for providing facilities to undertake resistivity and ultrasonic velocity measurements.

References

[1] E. Dagotto, T. Hotta, A. Moreo (2001) *Phys. Rep.* **344** 1.
[2] Y. Tokura (2006) *Rep. Prog. Phys.* **69** 797.
[3] T. Hatano (2013) *Sci. Rep.* **3** 2904.
[4] S. Jin, H. Tiefel, M. Mc Cornack, R.A. Fastnacht, R. Ramesh, L.H. Chen (1994) *Science* **264** 413.
[5] C. Autret, A. Maignan, C. Martin, M. Hervieu, V. Hardy, S. Hébert, B. Raveau (2003) *Appl. Phys. Lett.* **82** 4746.
[6] B. Raveau, A. Maignan, C. Martin (1997) *J. Solid State Chem.* **130** 162.
[7] T. Kimura, Y. Tomioka, Y. Okimoto, Y. Tokura (1999) *Phys. Rev. Lett.* **83** 3940.
[8] J.J.U. Buch, G. Lalitha, T.K. Pathak, N.H. Vasoya, V.K. Lakhani, P.V. Reddy, Ravi Kumar, K.B. Modi (2008) *J. Phys. D: Appl. Phys*. **41** 025406.
[9] G. Lalitha, D. Das, D. Bahadur, P. Venugopal Reddy (2008) *J. Alloys Compd* **464** 6.
[10] G. Lalitha Reddy, Y. Kalyana Lakshmi, N. Pavan kumar, S. Manjunath Rao, P. Venugopal Reddy (2001) *J. Magn. Magn. Mater.* **115** 1550.

[11] Y.V. Ramana, P. Venugopal Reddy (1989) *Acoust. Lett*. **13** 83.

[12] R.A. Young (1993) Introduction to the Rietveld Method, In: "*The Rietveld method*", ed. by R.A. Young (Oxford University Press, Oxford), pp. 1-38.

[13] E. Jansen, W. Schafer, G. Will (1994) *J. Appl. Cryst.* **27** 492.

[14] G. Lalitha, N. Pavan Kumar, P. Venugopal Reddy (2018) *J. Low Temp. Phys.* **192** 133.

[15] Lu Chengliang, Hu Ni, Ming Yang, Shuangcheng Xia, Haowen Wang, Junfeng Wang, Zhengcai Xia (2014) *Sci. Rep.* **4** 4902.

[16] G. Lalitha, P. Venugopal Reddy (2009) *J. Phys.: Condens. Matter* **21** 056003.

[17] R. Baldev, V. Rajendran, P. Palanichamy (2004) "*Science and Technology of Ultrasonics* (New Delhi: Narosa Publishing House).

[18] G. Lalitha, P. Venugopal Reddy (2009) *J. Phys. Chem. Sol.* **70** 960.

[19] D.P.H. Hasselman, R.M.J. Fulrath (1964) *J. Am. Ceram. Soc.* **47** 52.

[20] O.L. Anderson (1965) In: W.P. Mason (Ed.), "*Physical Acoustics*", vol. IIIB (Academic Press), p. 43.